Results in Engineering 27 (2025) 106230

Contents lists available at ScienceDirect

Results in Engineering

journal homepage: www.sciencedirect.com/journal/results-in-engineering

Research paper

An insight into the CO_2 solubility in NaCl + ethylene glycol (1:16) deep eutectic solvent: experimental and modeling

Ali Rasoolzadeh [a], Mehdi Keshtkar [b], Sona Raeissi [b,*], Reza Haghbakhsh [c,*]

[a] Department of Chemical Engineering, Faculty of Engineering, Behbahan Khatam Alanbia University of Technology, Behbahan, Iran
[b] School of Chemical and Petroleum Engineering, Shiraz University, Mollasadra Ave., Shiraz 71348-51154, Iran
[c] LAQV, REQUIMTE, Departamento de Química da Faculdade de Ciências e Tecnologia, Universidade Nova de Lisboa, 2829-516 Caparica, Portugal

ARTICLE INFO

Keywords:
Vapor–liquid equilibria
Green solvent
Thermodynamic modeling
Carbon dioxide
Carbon capture

ABSTRACT

The regulation of CO_2 emissions from industrial operations is crucial from an environmental perspective. The most widely used solvents for CO_2 capture consist of aqueous alkanolamine solutions. However, amine-based processes face several challenges, such as corrosion, chemical degradation, and high energy requirements for solvent regeneration. As potential alternatives, deep eutectic solvents (DESs) have emerged as promising eco-friendly and biodegradable options for CO_2 capture. This study experimentally measures the solubility of CO_2 in a DES (1 mol NaCl + 16 mol ethylene glycol) using a high-pressure solubility apparatus at the four temperatures of 293.15, 303.15, 313.15, and 323.15 K. For the thermodynamic modeling, the Soave Redlich Kwong equation of state (SRK EoS) was employed, coupled with three different mixing rules of van der Waals (vdW), Wong Sandler (WS), and modified Huron-Vidal (MHV1). The vdW approach was considered in the three cases without using binary interaction, constant binary interaction, and variable binary interaction parameter by temperature. The results demonstrated that by incorporating the WS and MHV1, the local composition concept was successful in addressing the non-ideality of the liquid phase. Among the tested models, the WS (AARD%= 6.66) and MHV1 (AARD%=5.61) provided the most accurate predictions of equilibrium pressures. Additionally, Henry's constant, standard Gibbs energy, enthalpy, and entropy of gas solvation were determined using the experimental data together with classical thermodynamic relations. The calculated negative standard enthalpy of solvation indicates an exothermic gas solvation process, signifying that energy is released as CO_2 dissolves in this DES.

1. Introduction

To minimize pollution resulting from the continued use of fossil fuels, it is essential to regulate CO_2 emissions from industrial processes and power plants. Three primary approaches are commonly used for CO_2 capture are pre-combustion, post-combustion, and oxyfuel combustion [1–3]. In the post-combustion process, suitable solvents or sorbents capture CO_2 from flue gases, followed by CO_2 separation and compression for storage [4,5]. The most widely used solvents for CO_2 capture are aqueous alkanolamine solutions. However, amine-based processes present several drawbacks, including corrosion, degradation, and high energy consumption for regeneration [6–8]. To overcome these challenges, physical solvents such as dimethylformamide (DMF) and polyethylene glycol (PEG) can serve as alternatives to amines, but they have lower absorption capacities [9,10]. Ionic liquids (ILs), another class of solvents suggested for this purpose, offer advantages such as tunable properties and low volatility, yet their high cost remains a limitation [11–14]. Nowadays, deep eutectic solvents (DESs) show interesting performances as eco-friendly and biodegradable alternatives to amines for CO_2 capture. Similar to ILs, DESs possess tunable physicochemical properties [15–17]. Furthermore, DESs exhibit several other superior characteristics, including low volatility, low toxicity, non-flammability, and high solubilizing capacity for a wide range of compounds. These properties make them valuable for applications as green solvents, electrolytes, and catalysts [18–21].

DESs are formed by mixing hydrogen bond acceptors (HBAs) and hydrogen bond donors (HBDs) in particular molar ratios, significantly lowering their melting points with respect to the individual constituent components. Strong hydrogen bonding between the HBD and HBA stabilizes the liquid phase, forming a three-dimensional hydrogen bond

* Corresponding authors.
E-mail addresses: raeissi@shirazu.ac.ir (S. Raeissi), r.haghbakhsh@fct.unl.pt (R. Haghbakhsh).

https://doi.org/10.1016/j.rineng.2025.106230
Received 2 May 2025; Received in revised form 7 July 2025; Accepted 9 July 2025
Available online 9 July 2025

network. The chemical structures of the HBDs and HBAs influence the strength of hydrogen bonding; thus, a calculated choice of their types and ratios enables the customization of DES properties for specific applications.

When a DES is employed for CO_2 capture, multiple intermolecular forces contribute to the absorption mechanism, including hydrogen bonding between CO_2 and the HBA groups of the DES, as well as van der Waals forces between CO_2 and DES components. Most thermodynamic models for the computation of CO_2 solubility have treated a DES as a pseudo-compound. With this perspective, selecting an appropriate thermodynamic model is crucial for accurate solubility predictions [22,23]. Al-Bodour et al. provided a comprehensive review of CO_2 solubility in DESs [24].

This study experimentally measures the solubility of CO_2 in the DES consisting of 1 NaCl + 16 ethylene glycol using a high pressure validated equipment at different temperatures. For the thermodynamic modeling, the φ-φ approach is applied, wherein fugacity coefficients are computed using the Soave Redlich Kwong (SRK EoS) [25] coupled with three different mixing rules of van der Waals (vdW) [26], Wong-Sandler (WS) [27,28], and modified Huron-Vidal (MHV1) [29]. The vdW mixing rules were considered in three modes [30–32]. With (k_{ij}=0), with (k_{ij}=k), and with (k_{ij}=k_1T+k_2). The WS and MHV1 mixing rules are utilized to examine the impact of the local composition concept on intermolecular forces in the CO_2/DES system. These mixing rules were coupled with the non-random two-liquid (NRTL) model. The Henry's constant (H_i), standard solvation Gibbs energy (ΔG^0_{sol}), standard solvation (ΔH^0_{sol}), and standard solvation entropy (ΔS^0_{sol}) are also determined using the experimental data and classical thermodynamic relations.

2. Experimental

2.1. Materials

Table 1 outlines the chemicals employed in this work, together with their purities and suppliers.

The synthesis of the DES involved drying the HBA and HBD, followed by accurately weighing them to achieve a HBA:HBD molar ratio of 1:16 using a high accuracy balance (sensitivity of 0.001 g), then the weighed HBD and HBA were stirred and mixed in a closed top flask and subjected for strong shaking in a shaker incubator at 60 °C for 24 h. After achieving a uniform and colorless liquid DES, in order to minimize moisture content, the synthesized DES was transferred to a vacuum oven for an additional 24 h at a temperature of 60 °C. Finally, the dried DES's water content was measured with a Karl-Fischer titrator, yielding a mass fraction of 0.0001. The formation of a deep eutectic solvent (DES) from the mixture of sodium chloride and ethylene glycol at a molar ratio of 1:16 has been confirmed in the literature [33].

The final dried synthesized DES was used for carbon dioxide absorption experiments in a high gas solubility measurement apparatus, which has been validated before in published studies. The details of the experiment and measurement apparatus were published before [18,22,23]. Further details about methodology and procedural framework for measuring CO_2 solubility, the specifications of the measuring instruments, along with their associated uncertainties, and the method of evaluation of the uncertainties of the CO_2 mole fractions were presented in the Supporting Information section.

Table 1
The list of chemicals used with their vendors and purities in this work.

Material	CAS number	Supplier	Initial purity[a]	Purification method
Sodium chloride	7647–14–5	Merck	99.5 %	Dried 24 h in a vacuum oven
Ethylene glycol	107–21–1	Merck	99.5 %	Dried 24 h in a vacuum oven
Carbon dioxide	124–38–9	Tarkib Gas Pars	99.995 %	No further purification

[a]mass fraction.

3. Thermodynamic modeling

The SRK EoS [25], in combination with the vdW [26], WS [27,28], and MHV1 mixing rules [29] was employed to calculate the equilibrium pressures of the CO_2 + DES system. Among these models, the vdW mixing rules were the most simple, the MHV1 mixing rules exhibited moderate complexity, while the WS mixing rules were the most complex, providing a detailed representation of the non-ideality of the liquid phase. The SRK EoS is expressed as follows [25]:

$$P = \frac{RT}{v-b} - \frac{a}{v(v+b)} \tag{1}$$

In Eq. (1), P denotes the absolute pressure, T represents the absolute temperature, R signifies the universal gas constant, and v corresponds to the molar volume. The parameters a and b describe attractive and repulsive forces, respectively. The temperature dependence of the attraction parameter a is expressed as follows [25]:

$$a = \left[1 + \left(0.48 + 1.574\omega - 0.176\omega^2\right)\left(1 - T_r^{0.5}\right)\right]^2 \left(0.42747 \frac{R^2 {T_c}^2}{P_c}\right) \tag{2}$$

In Eq. (2), P_c and T_c represent the critical pressure and critical temperature, respectively. The parameter ω denotes the acentric factor, which characterizes the deviation of a substance from idealized spherical molecules. It is worth mentioning that DES was assumed to be a pseudo-component. The reduced temperature, T_r, is defined as the ratio of the temperature to the critical temperature. The repulsion parameter is expressed as follows:

$$b = 0.08664 \frac{RT_c}{P_c} \tag{3}$$

The cubic representation of the SRK EoS in terms of compressibility factor (Z) is given by [25],

$$Z^3 - Z^2 + \left(A - B - B^2\right)Z - (AB) = 0 \tag{4}$$

where, A and B are dimensionless parameters:

$$A = \frac{aP}{R^2T^2} \tag{5}$$

$$B = \frac{bP}{RT} \tag{6}$$

Finally, the fuacity coefficient (φ_i) for the SRK EoS is defined as follows [25]:

$$Ln\varphi_i = (Z-1) - \mathrm{Ln}(Z-B) - \frac{A}{B}\mathrm{Ln}\left(1 + \frac{B}{Z}\right) \tag{7}$$

The parameters a and b of the mixture can be determined using the combination of the SRK EoS and the aforementioned mixing rules. The simplest approach for calculating these parameters is through the vdW mixing rules, which are expressed as follows [26].

$$a_{mix} = \sum_{i=1}^{n}\sum_{j=1}^{n} x_i x_j \left(a_i a_j\right)^{0.5}\left(1 - k_{ij}\right) \tag{8}$$

$$b_{mix} = \sum_{i=1}^{n} x_i b_i \tag{9}$$

According to Eqs. (8) and (9), a_{mix} exhibits a quadratic dependence on the mole fractions, whereas b_{mix} follows a linear dependence. The binary interaction parameter (BIP) between components ii and jj is denoted by k_{ij}.

The vdW mixing rules were applied in three distinct scenarios: with (k_{ij}=0), with (k_{ij}=k), and with (k_{ij}=k_1T+k_2). The WS and MHV1 mixing rules were employed to analyze the impact of local composition on intermolecular interactions within the CO_2/DES system. These models incorporated the appropriate G^{Excess} model to account for liquid-phase non-idealities. While the MHV1 model employed the same relation for b_{mix} as the vdW mixing rules, it introduced a new formulation for the dimensionless mixture parameter α_{mix} [29].

$$\alpha_{mix} = \sum_i x_i \alpha_i + \frac{1}{q_1}\left(\frac{G^{Excess}}{RT} + \sum_i x_i ln\frac{b}{b_i}\right) \tag{10}$$

$$\alpha = \frac{a}{bRT} \tag{11}$$

In Eq. (10), q_1 is an EoS-dependent constant. For the SRK EoS, q_1 has a value of −0.593 [29] Finally, the most complex mixing rules, the WS mixing rules, were applied to account for the non-ideality of the liquid phase and improve the accuracy of the CO_2 solubility predictions [27,28]:

$$a_{mix} = RT\frac{\left(\sum_i\sum_j x_i x_j\left(b-\frac{a}{RT}\right)_{ij}\right)\left(\sum_i x_i\left(\frac{a_i}{b_i RT}\right)\right) + \left(\frac{G^{Excess}}{CRT}\right)}{1-\left(\sum_i x_i\left(\frac{a_i}{b_i RT}\right)\right) - \left(\frac{G^{Excess}}{CRT}\right)} \tag{12}$$

$$b_{mix} = \frac{\left(\sum_i\sum_j x_i x_j\left(b-\frac{a}{RT}\right)_{ij}\right)}{1-\left(\sum_i x_i\left(\frac{a_i}{b_i RT}\right)\right) - \left(\frac{G^{Excess}}{CRT}\right)} \tag{13}$$

In Eqs. (12) and (13), $\left(b-\frac{a}{RT}\right)_{ij}$ represents the second virial coefficient and has the following relation [27,28]:

$$\left(b-\frac{a}{RT}\right)_{ij} = \frac{b_i+b_j}{2} - \frac{(a_i a_j)^{0.5}(1-k_{ij})}{RT} \tag{14}$$

In Eqs. (12) and (13), C is a parameter for the EoS. For the SRK EoS, C is −0.69315 [27,28]. Compared to the MHV1 model, the WS model includes an additional optimizing parameter, k_{ij}, which enhances its flexibility in correlating experimental data. For both G^{Excess} mixing rules (MHV1 and WS), the NRTL G^{Excess} model was employed to account for the non-ideality of the liquid phase [34–36].

$$\frac{G^{Excess}}{RT} = x_1 x_2\left(\frac{\tau_{21}G_{21}}{x_1+x_2G_{21}} + \frac{\tau_{12}G_{12}}{x_2+x_1G_{12}}\right) \tag{15}$$

$$\tau_{12} = \frac{g_{12}-g_{22}}{RT} \tag{16}$$

$$\tau_{21} = \frac{g_{21}-g_{11}}{RT} \tag{17}$$

$$G_{12} = \exp(-\alpha'\tau_{12}) \tag{18}$$

$$G_{21} = \exp(-\alpha'\tau_{21}) \tag{19}$$

The binary parameters of $g_{12-}g_{22}$ and $g_{21-}g_{11}$ represent the interaction energies. α' stands for the non-randomness parameter and has values ranging from 0.20 to 0.49 [35].

For dilute liquid mixtures, the Henry's constant for a solute i is thermodynamically defined as follows [18,22,23]:

$$H_i = \lim_{x_i\to 0}\left(\frac{f_i^{liq}}{x_i}\right) \tag{20}$$

In this expression, H_i stands for the Henry's constant of component i, while f_i^{liq} and x_i represent the fugacity and mole fraction of solute i in the liquid phase, respectively. To assess this limit behavior, the condition of phase equilibrium, where fugacities of the component in both vapor and liquid states are equal, is employed. This condition can be expressed using a modified form of Raoult's Law in the following equations.

$$f_i^{liq} = f_i^{vap} = y_i P\phi_i^{Vap} \tag{21}$$

$$H_i = \lim_{x_i\to 0}\left(\frac{f_i^{liq}}{x_i}\right) = \lim_{x_i\to 0}\left(\frac{f_i^{vap}}{x_i}\right) = \lim_{x_i\to 0}\left(\frac{y_i\varphi_i^{vap}P}{x_i}\right) = \lim_{x_i\to 0}\left(\frac{P}{x_i}\right) \tag{22}$$

Here, P is the total system pressure, y_i is the vapor phase mole fraction of species i, and ϕ_i^{Vap} is the fugacity coefficient in the vapor phase. The derivation of Eq. (22), showing that Henry's constant corresponds to the tangent of the pressure-composition curve at infinite dilution, requires two simplifying assumptions. First, it assumes that the solvent (DES) has negligible vapor pressure, which is valid since DESs typically exhibit extremely low volatility. Second, the vapor-phase fugacity coefficient is approximated to be unity [18,22]. This is a fair approximation given that the system pressures used (up to 3.6 MPa) and temperatures (no lower than 293.2 K) are within the range where CO_2 behaves nearly ideally in the vapor phase. Once H_i is known, it becomes straightforward to evaluate the associated standard thermodynamic functions of the standard entropy of dissolution ΔS^0_{sol}, standard enthalpy of dissolution ΔH^0_{sol}, and the standard Gibbs energy of dissolution ΔG^0_{sol}. These are calculated using the following equations:

$$\Delta G^0_{sol} = RT\mathrm{Ln}\left(\frac{H_i}{P^0}\right) \tag{23}$$

$$\Delta H^0_{sol} = R\left(\frac{\partial\left(\mathrm{Ln}\left(\frac{H_i}{P^0}\right)\right)}{\partial\left(\frac{1}{T}\right)}\right)_P \tag{24}$$

$$\Delta S^0_{sol} = \left(\frac{\Delta H^0_{sol} - \Delta G^0_{sol}}{T}\right) \tag{25}$$

where P^0 is the standard reference pressure, typically taken as 0.1 MPa. Each of those thermodynamic parameters provides key insights. ΔS^0_{sol} reflects the degree of disorder or randomness introduced by the solvation process, ΔH^0_{sol} represents the thermal effect of dissolution, whether heat is absorbed or released, and ΔG^0_{sol} indicates the system's energetic favorability at equilibrium, as systems tend to minimize their Gibbs free energy [18,22,23,37–39].

4. Results and discussion

The experimental isothermal pressure-mole fraction (P-x) data for the CO_2 (1) + DES (1 NaCl + 16 ethylene glycol) (2) system are presented in Table 2. This table also includes the uncertainties associated with the measured mole fractions.

According to Table 2, the typical trend in gas solubility in solvents is observed, where CO_2 solubility decreases with increasing temperature. Raising the temperature reduces gas solubility due to the increased molecular motion, which weakens intermolecular interactions. A comparison of the experimental isothermal P-x data for the system CO_2 (1) + 1 NaCl + 16 ethylene glycol (2) is presented in Fig. 2, illustrating the effects of not only temperature, but also pressure. At a fixed temperature, according to Fig. 1, an increase in pressure results in enhanced solubility of CO_2 in the DES across all isotherms, consistent with Henry's law. For the investigation of the effect of NaCl presence, a comparative analysis was carried out between the investigated DES and the available experimental data for pure ethylene glycol reported in the literature. As shown in Fig. S1 in the Supporting Information, the solubility of CO_2 is plotted as a function of pressure, covering a range up to approximately 7 MPa. According to this figure, CO_2 solubility values of the investigated DES closely follow the same trend and magnitude observed for pure

Table 2
Isothermal solubility (mole fraction) data and their uncertainties for CO_2 (1) + 1 NaCl + 16 ethylene glycol (2).

T / K	P / MPa	x_1	$\frac{u(x_1)}{x_1}$	T / K	P / MPa	x_1	$\frac{u(x_1)}{x_1}$
293.2	0.4156	0.0068	0.0215	313.2	0.4521	0.0048	0.0397
	0.8656	0.0159	0.0236		0.9453	0.0117	0.0218
	1.3618	0.0252	0.0180		1.4913	0.0190	0.0168
	1.7613	0.0345	0.0162		1.9311	0.0278	0.0152
	2.1798	0.0452	0.0151		2.4006	0.0374	0.0142
	2.5763	0.0529	0.0145		2.8531	0.0426	0.0136
	3.0898	0.0614	0.0139		3.4398	0.0511	0.0131
303.2	0.4338	0.0058	0.0413	323.2	0.4688	0.0044	0.0383
	0.9043	0.0141	0.0227		0.9821	0.0106	0.0211
	1.4258	0.0223	0.0173		1.5531	0.0171	0.0162
	1.8473	0.0308	0.0156		2.0123	0.0257	0.0147
	2.2908	0.0411	0.0146		2.5116	0.0334	0.0138
	2.7161	0.0472	0.0141		2.9846	0.0401	0.0133
	3.2656	0.0560	0.0135		3.6086	0.0481	0.0127

Standard uncertainties u are u(T) = 0.2 K, u(P)= 0.0005 MPa and $\frac{u(x_1)}{x_1}$ is the relative uncertainty of the CO_2 mole fraction.

ethylene glycol with no significant enhancement. This comparison clearly suggests that the presence of NaCl at a low molar ratio (1:16) does not lead to a meaningful increase in CO_2 solubility under the studied conditions. Since NaCl is a non-volatile inorganic salt with limited interaction with gaseous CO_2, its influence is likely restricted to subtle effects on the bulk properties of the solvent, such as polarity or hydrogen bonding network. Thus, the CO_2 solubility behavior is primarily governed by ethylene glycol.

The equilibrium pressures of this CO_2 + DES system were calculated using the SRK EoS in combination with three different mixing rules. However, due to the lack of available data for the critical properties and acentric factor of NaCl + 16 ethylene glycol, considered as one pseudo-component, existing experimental liquid density data for NaCl + 16 ethylene glycol [33] was utilized to obtain these parameters by optimization using the SRK EoS. Table 3 presents the critical properties and acentric factors for CO_2 and the pseudo-component representing the DES, which were employed in the thermodynamic modeling.

Next, the parameters of the mixing rules were optimized using the following objective function:

$$O.F = (AARD)_P(\%) = \frac{100}{Number\ of\ Data} \times \sum \frac{|P_{Exp} - P_{Cal}|}{P_{Exp}} \quad (26)$$

Table 4 presents the optimized parameters for the vdW, MHV1, and WS mixing rules.

For all the systems, α was considered as a constant value of 0.3. The $(AARD)_P(\%)$ of the calculated equilibrium pressures for all the models are demonstrated in Table 5.

According to Table 5, the absence of any binary interaction parameters in the vdW mixing rule resulted in very poor predictions of equilibrium pressures, with an average absolute relative deviation $(AARD)_P\%$ of 76.48 %. This finding highlights the significant role of the interaction parameter (k_{ij}) in such a system. Furthermore, Table 5 reveals that both constant k_{ij} ($(AARD)_P\%$= 12.75 %) and temperature-dependent k_{ij} ($(AARD)_P\%$= 6.97 %) models produced close results. This indicates that incorporating temperature dependence for the k_{ij} significantly enhances the model's estimation capability. The *AARD%* obtained for the SRK with temperature-dependent k_{ij} is comparable to those achieved using the SRK + WS + NRTL and SRK + MHV1+ NRTL. The WS ($(AARD)_P\%$= 6.66 %) and MHV1 ($(AARD)_P\%$= 5.61 %) models yielded the most accurate equilibrium pressures for this binary system. Ultimately, it was concluded that the application of the WS and MHV1 Gexcess models, alongside the local composition concept, effectively addressed the non-ideality of the liquid phase. Figs. 2-5 present a comparison between the experimental and calculated *P-x* data for the CO_2 +

Table 3
The critical pressures (P_c), critical temperatures (T_c) and acentric factors (ω) of CO_2 [33,40] and the DES.

Component	T_c (K)	P_c (MPa)	ω
CO_2	304.21	7.383	0.2236
1 NaCl + 16 ethylene glycol	538.90	8.550	0.5631

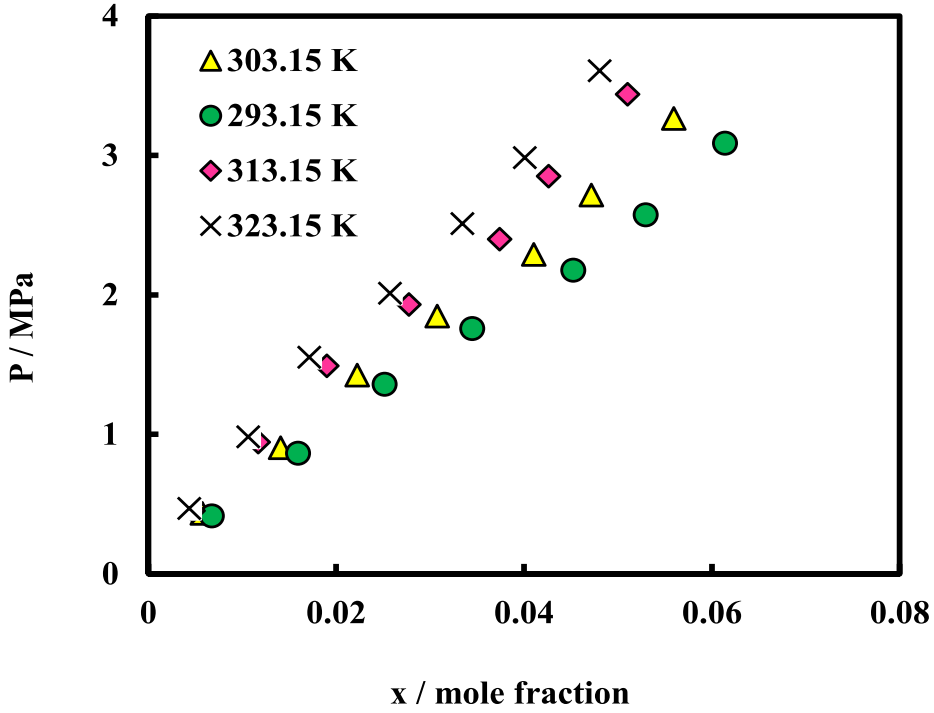

Fig. 1. Experimentally determined *P-x* data of CO_2 in 1 NaCl + 16 ethylene glycol at four different temperatures.

Table 4
The optimized parameters of the vdW, MHV1, and WS for CO_2 (1) + 1 NaCl + 16 ethylene glycol (2).

Model	Optimized parameters		
SRK + vdW ($k_{1ij} = k$)	k		
	0.167913		
SRK + vdW ($k_{ij} = k_1 T + k_2$)	k_1 (K^{-1})	k_2	
	0.001043	−0.151828	
SRK + WS + NRTL	$g_{12}-g_{22}$ ($J.mol^{-1}$)	$g_{21}-g_{11}$ ($J.mol^{-1}$)	k_{ij}
	−25,065.49	2996.50	−0.0999
SRK + MHV1 + NRTL	$g_{12}-g_{22}$ ($J.mol^{-1}$)	$g_{21}-g_{11}$ ($J.mol^{-1}$)	
	−31,209.45	3136.58	

Table 5
$(AARD)_P$(%) for the calculated equilibrium pressures of the system of CO_2 (1) + 1 NaCl + 16 ethylene glycol (2).

Model	NDP[a]	$(AARD)_P$ (%)
(SRK + vdW) with $k_{ij} = 0$	28	76.48
(SRK + vdW) with $k_{ij} = k$	28	12.75
(SRK + vdW) with $k_{ij} = k_1 T + k_2$	28	6.97
(SRK + WS + NRTL)	28	6.66
(SRK + MHV1+ NRTL)	28	5.61

[a]number of data points.

1 NaCl + 16 ethylene glycol system.

As illustrated in Figs. 2–5, the WS and MHV1 mixing rules yielded the most accurate results at lower concentrations. Furthermore, the accuracy of the vdW mixing rules with the binary interaction parameter improved as the temperature increased. This is attributed to the reduction in the non-ideality of the liquid phase at higher temperatures. For a statistical evaluation of the calculated results, the error scattering for the most accurate thermodynamic combination (SRK + MHV1 + NRTL) is shown in Fig. 6, and the cross plot in Fig. 7.

The results presented in Figs. 6 and 7 demonstrate that the thermodynamic combination of SRK + MHV1 + NRTL produced excellent results for the equilibrium pressures of the CO_2 + (1 NaCl + 16 ethylene glycol).

Following the phase equilibrium calculations, H_i, ΔG^0_{sol}, ΔH^0_{sol}, and ΔS^0_{sol} were calculated. The results are presented in Table 6.

Table 6 shows that an increase in temperature was associated with higher values of H_1, corresponding to the fact that increasing the temperature reduces the solubility of CO_2 in the DES. The positive values of the standard Gibbs free energy of solvation (ΔG^0_{sol}) reflect an unfavorable tendency for CO_2 to dissolve in the 1 NaCl + 16 ethylene glycol DES under standard conditions. However, it is important to note that ΔG^0_{sol} represents the affinity or thermodynamic tendency between the pure components and does not alone determine spontaneity. The actual criterion for spontaneity is the Gibbs free energy change (ΔG), given by $\Delta G = \Delta G^\circ + RT \ln x$, where x is the mole fraction of CO_2 in the solvent. As temperature increases, the values of ΔG^0_{sol} also increase, suggesting a decreasing thermodynamic affinity and reduced solubility of CO_2 in the DES at higher temperatures. Additionally, the negative values of ΔH^0_{sol} suggest that energy is released during the dissolution process, making it exothermic. Therefore, affirming the experimentally observed trend that the solubility of CO_2 in the DES is greater at lower temperatures. Finally, the negative values of ΔS^0_{sol} indicate that the dissolution process leads to a reduction in disorder.

As the final discussion, it is important to note that to enhance the understanding of the underlying mechanism governing CO_2 solubility in deep eutectic solvents (DESs), it is scientifically meaningful to analyze the relationship between the entropy of gas dissolution and the available free or void volume in the solvent matrix. As suggested by recent studies [41,42], the void volume can be quantitatively estimated using experimentally accessible properties such as the molar volume and refractive index of the DESs. These parameters offer insight into the packing efficiency and microstructural free space within the solvent, which in turn influence gas dissolution behavior. By establishing this correlation, it becomes possible to distinguish the relative entropic versus enthalpic contributions to the overall solvation thermodynamics. Such analysis not only provides molecular-level interpretation of gas–solvent

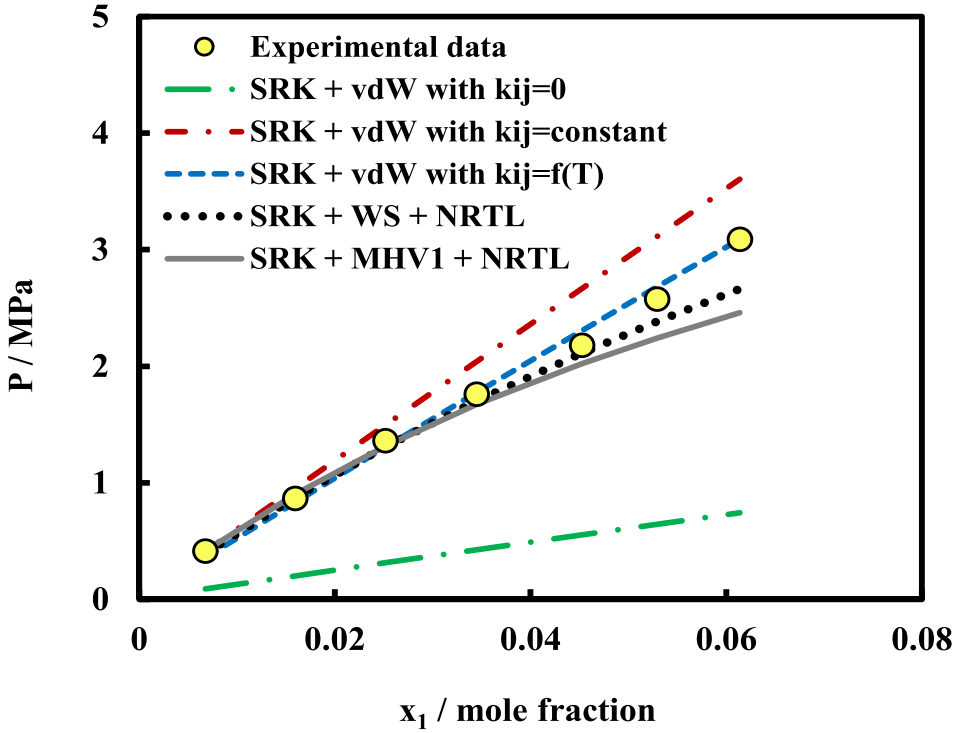

Fig. 2. *P-x* data of CO_2 (1) + 1 NaCl + 16 ethylene glycol (2) at $T = 293.15$ K.

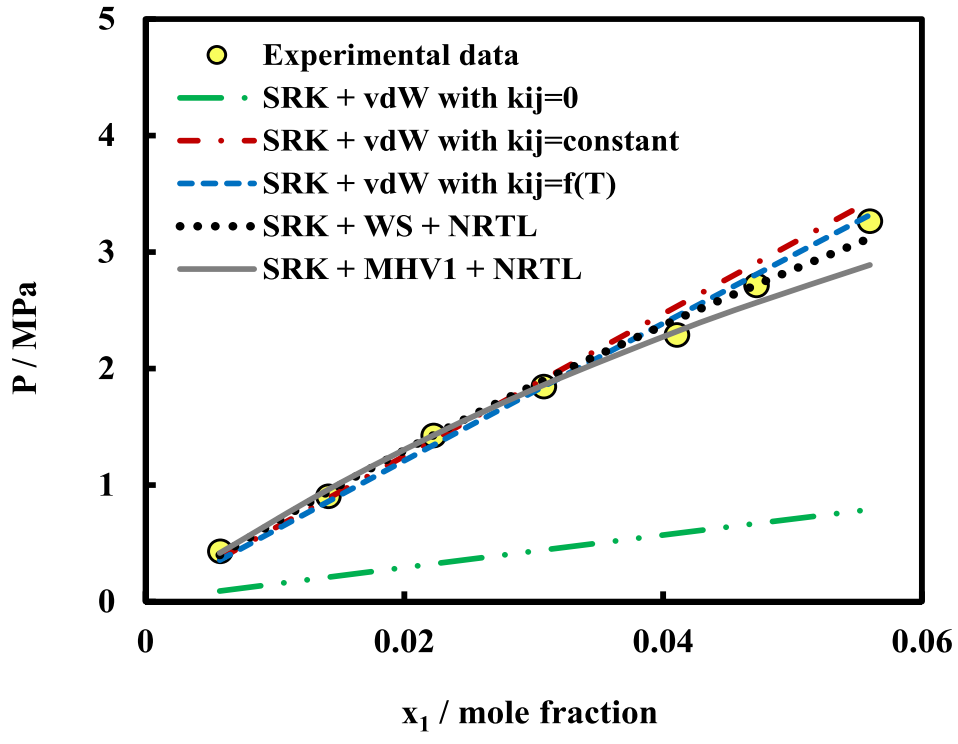

Fig. 3. *P-x* data of CO_2 (1) + 1 NaCl + 16 ethylene glycol (2) at $T = 303.15$ K.

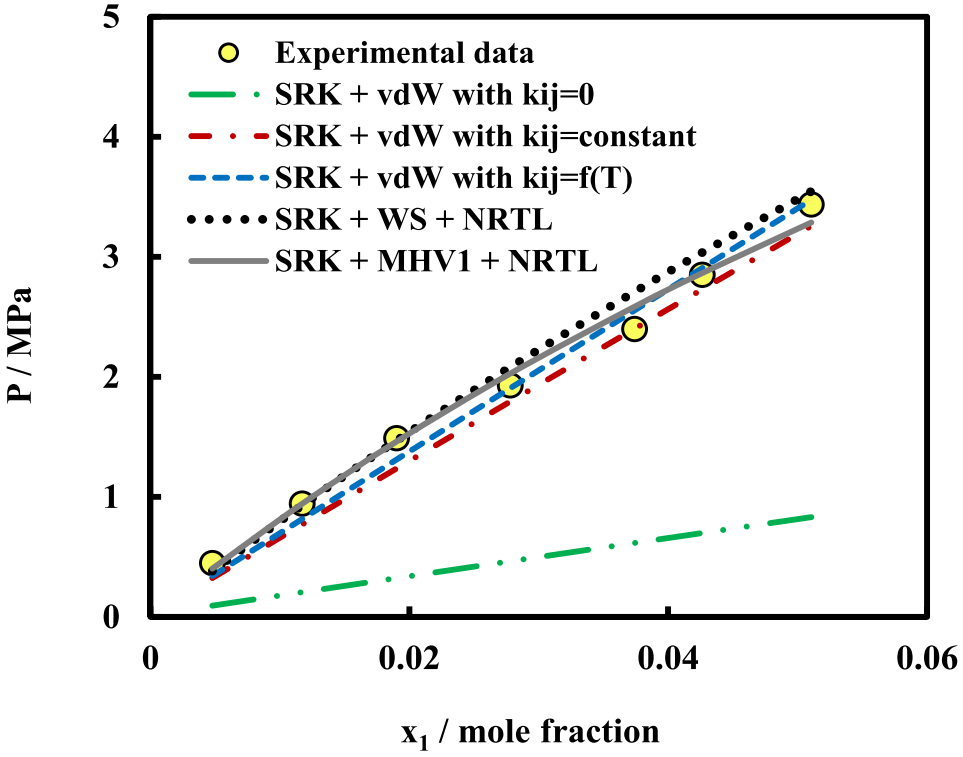

Fig. 4. *P-x* data of CO_2 (1) + 1 NaCl + 16 ethylene glycol (2) at $T = 313.15$ K.

interactions but also supports the rational design of DESs with enhanced CO_2 capture performance through entropic optimization.

5. Conclusions

Deep eutectic solvents are considered promising alternatives to amines for CO_2 capture due to their advantageous properties. They have low vapor pressures, making them less volatile and more environmentally friendly compared to traditional organic solvents. Additionally, they exhibit reduced toxicity, making them safer for handling and application. This study aimed to experimentally measure the solubility of CO_2 in the DES (1 NaCl + 16 ethylene glycol) across four isotherms:

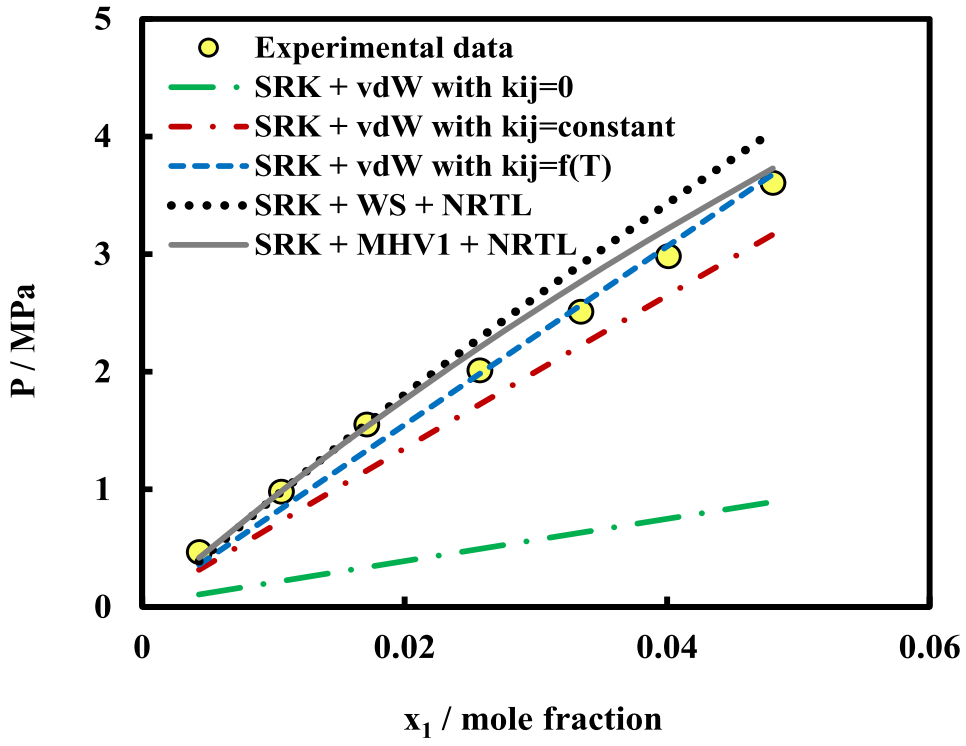

Fig. 5. *P-x* data of CO_2 (1) + 1 NaCl + 16 ethylene glycol (2) at $T = 323.15$ K.

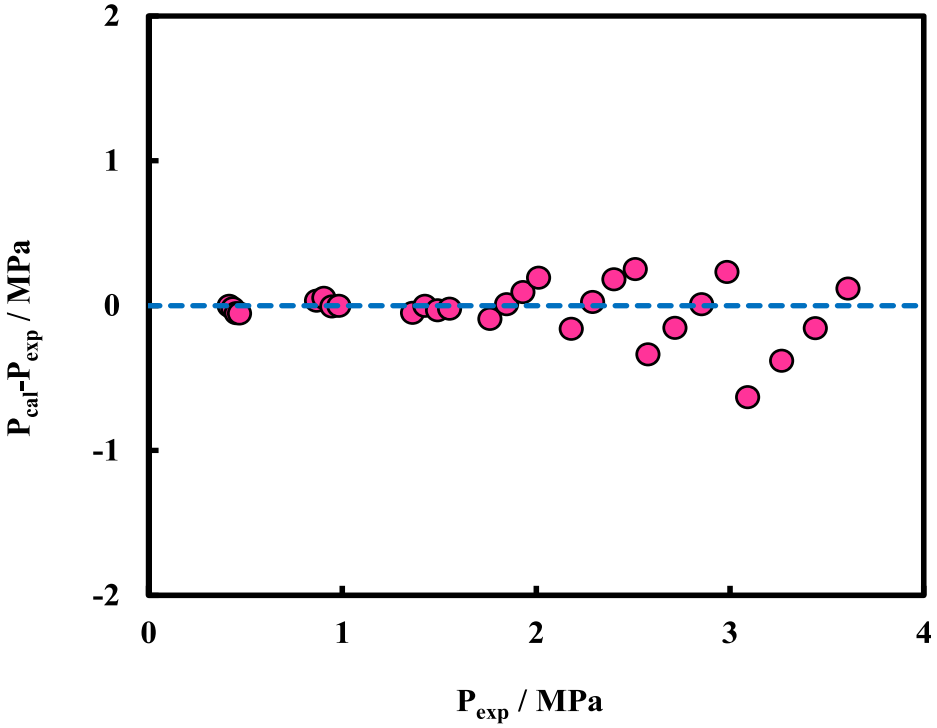

Fig. 6. Difference between the calculated (SRK + MHV1 + NRTL) and experimental equilibrium pressures vs. experimental equilibrium pressures for all of the data points.

293.15, 303.15, 313.15, and 323.15 K, with pressures ranging up to around 3 MPa. The solubility of CO_2 in this DES was calculated using the combination of the SRK EoS and three mixing rules: vdW, WS, and the MHV1. The vdW mixing rule was applied in three cases: with ($k_{ij} = 0$), with (k_{ij}=k), and with ($k_{ij} = k_1T+k_2$). The absence of a binary interaction parameter in the vdW mixing rule led to inaccurate predictions of equilibrium pressures, resulting in the $(AARD)_P\%$ of 76.48 %. This highlights the critical role of k_{ij} in this binary system. Furthermore, the use of a constant k_{ij} ($(AARD)_P\% = 12.75$ %) or a temperature-dependent k_{ij} ($(AARD)_P\% = 6.97$ %) yielded close results. The application of the WS ($(AARD)_P\% = 6.66$ %) and MHV1 ($(AARD)_P\%$=5.61 %) Gexcess models, combined with the local composition concept, successfully addressed

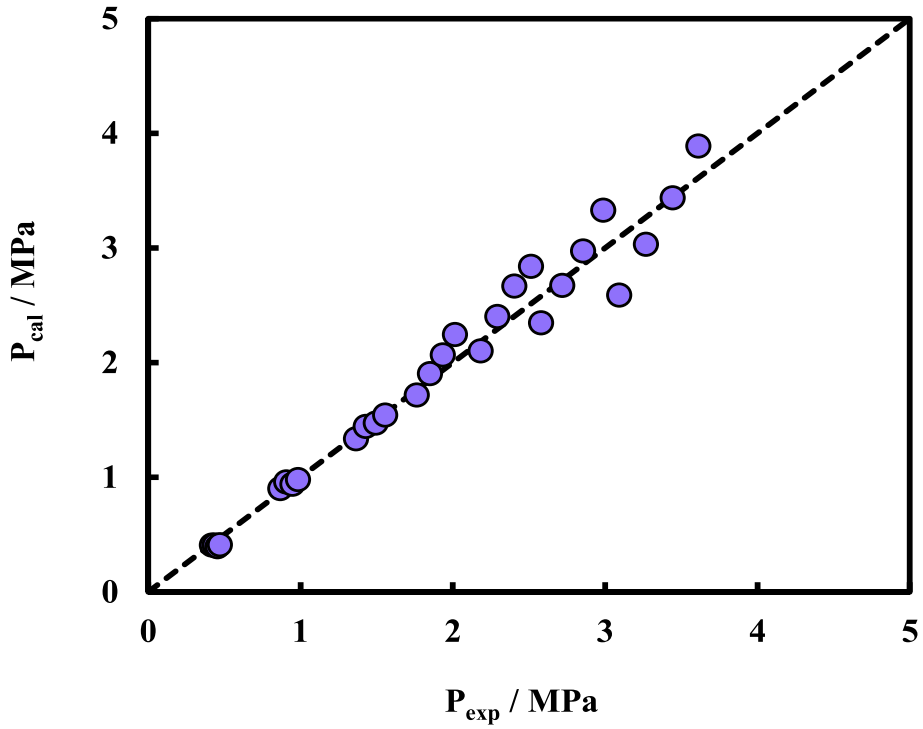

Fig. 7. Cross plot of experimental equilibrium pressures vs. the corresponding calculated (SRK + MHV1 + NRTL) values.

Table 6
The computed values of H_1, ΔG^0_{sol}, ΔH^0_{sol}, and ΔS^0_{sol} for the system of CO_2 (1) in 1 NaCl + 16 ethylene glycol (2).

	$T = 293.15$ K	$T = 303.15$ K	$T = 313.15$ K	$T = 323.15$ K
H_1 (MPa)	474.64	550.00	622.37	695.59
$\Delta G^0_{sol}\left(\text{kJ.mol}^{-1}\right)$	15.02	15.90	16.75	17.58
$\Delta H^0_{sol}\left(\text{kJ.mol}^{-1}\right)$	−11.05	−10.23	−9.63	−9.17
$\Delta S^0_{sol}\left(\text{J.mol}^{-1}\text{K}^{-1}\right)$	−88.93	−86.22	−84.24	−82.79

the non-ideality of the liquid phase. Following the phase equilibrium calculations, H_i, ΔG^0_{sol}, ΔH^0_{sol}, and ΔS^0_{sol} were computed. An increase in temperature led to higher values of H_i and ΔG^0_{sol}, indicating a decrease in the solubility of CO_2 in DES. Finally, the negative values of ΔH^0_{sol} confirmed that energy is released during the dissolution process, making it exothermic.

Declaration of generative AI and AI-assisted technologies in the writing process

During the preparation of this work, the authors used Grammarly and ChatGPT in order to check the grammar and improve clarity. After using this tool/service, the authors reviewed and edited the content as needed and took full responsibility for the content of the publication.

CRediT authorship contribution statement

Ali Rasoolzadeh: Writing – original draft, Software, Methodology, Investigation, Formal analysis, Conceptualization. **Mehdi Keshtkar:** Investigation, Data curation, Conceptualization. **Sona Raeissi:** Writing – review & editing, Validation, Supervision, Project administration, Formal analysis, Conceptualization. **Reza Haghbakhsh:** Writing – review & editing, Supervision, Methodology, Funding acquisition, Formal analysis, Data curation, Conceptualization.

Declaration of competing interest

The authors declare that they have no known competing financial interests or personal relationships that could have appeared to influence the work reported in this paper.

Acknowledgment

The authors are grateful to Shiraz University for providing facilities. Also, the parts of the research which were carried out at Universidade Nova de Lisboa. This work was financed by national funds from FCT - Fundação para a Ciência e a Tecnologia, I.P., under the scope of the project UID/50006/2023 of the Associate Laboratory for Green Chemistry - LAQV REQUIMTE and through national funds by CEEC IND5ed (DOI 10.54499/2022.05803.CEECIND/CP1725/CT0003).

Supplementary materials

Supplementary material associated with this article can be found, in the online version, at doi:10.1016/j.rineng.2025.106230.

Data availability

Data will be made available on request.

References

[1] R. Wanison, P. Sripuangchai, P. Phermkorn, T. Soisuwan, N. Kammuang-lue, P. Terdtoon, N. Tippayawong, Y. Mona, P. Suttakul, P. Sakulchangsatjatai, Performance analysis of precooling systems for cryogenic carbon capture: a comparative study of theoretical, numerical, and experimental methods, Results Eng. 23 (2024) 102763.
[2] M.M.G. Perdana, R. Andika, B.H. Susanto, S. Steven, N. Nishiyama, I.C. Sophiana, Transforming CO_2 emissions into fuel: an energy analysis of dimethyl ether production pathways, Results Eng. 25 (2025) 104330.
[3] M. Kheirinik, S. Ahmed, N. Rahmanian, Comparative techno-economic analysis of carbon capture processes: pre-combustion, post-combustion, and oxy-fuel combustion operations, Sustainability 13 (2021) 13567.
[4] F. Hosseinifard, M. Setak, M. Amidpour, Integrating machine learning-based classification and regression models for solvent regeneration prediction in post-

combustion carbon capture: an absorption-based case, Results Eng. 26 (2025) 104856.
[5] S. Zhang, Y. Shen, L. Wang, J. Chen, Y. Lu, Phase change solvents for post-combustion CO2 capture: principle, advances, and challenges, Appl. Energy 239 (2019) 876–897.
[6] A.H. Moghaddam, M. Esfandyari, H. Sakhaeini, Optimization of amine-based carbon capture: simulation and energy efficiency analysis of absorption section, Results Eng. 24 (2024) 103574.
[7] V.O. Viola, T.F. de Aquino, S.T. Estevam, B. Bonetti, H.G. Riella, C. Soares, N. Padoin, Synthesis and application of two types of amine sorbents impregnated on silica from coal fly ash for CO_2 capture, Results Eng. 20 (2023) 101596.
[8] D. Galatro, M. Machavolu, G. Navas, Transfer learning strategies for neural networks: a case study in amine gas treating units, Results Eng. 24 (2024) 103027.
[9] Z.H. Ban, L.K. Keong, A.Mohd Shariff, Physical absorption of CO2 capture: a review, Adv. Mat. Res. 917 (2014) 134–143.
[10] R. Eshraghi, M. Fasihi, A. Ghaemi, Optimization of PEG-modified phenolic foam for enhanced CO_2 adsorption: a micro-meso structural approach, Results Eng. 26 (2025) 104864.
[11] S. Lian, C. Song, Q. Liu, E. Duan, H. Ren, Y. Kitamura, Recent advances in ionic liquids-based hybrid processes for CO2 capture and utilization, J. Environ. Sci. 99 (2021) 281–295.
[12] W.F. Elmobarak, F. Almomani, M. Tawalbeh, A. Al-Othman, R. Martis, K. Rasool, Current status of CO2 capture with ionic liquids: development and progress, Fuel 344 (2023) 128102.
[13] M. Aghaie, N. Rezaei, S. Zendehboudi, A systematic review on CO2 capture with ionic liquids: current status and future prospects, Renew. Sustain. Energy Rev. 96 (2018) 502–525.
[14] B. Kazmi, S.A.A. Taqvi, D. Juchelkov, G. Li, S.R. Naqvi, Artificial intelligence-enhanced solubility predictions of greenhouse gases in ionic liquids: a review, Results Eng. 25 (2025) 103851.
[15] N. Ahmad, X. Lin, X. Wang, J. Xu, X. Xu, Understanding the CO2 capture performance by MDEA-based deep eutectics solvents with excellent cyclic capacity, Fuel 293 (2021) 120466.
[16] N. Zhang, Z. Huang, H. Zhang, J. Ma, B. Jiang, L. Zhang, Highly efficient and reversible CO2 capture by task-specific deep eutectic solvents, Ind. Eng. Chem. Res. 58 (2019) 13321–13329.
[17] S. Foorginezhad, X. Ji, Enhanced CO_2 capture performance using deep eutectic solvent-immobilized silica slurry, Results Eng. 26 (2025) 105162.
[18] R. Haghbakhsh, M. Keshtkar, A. Shariati, S. Raeissi, Experimental investigation of carbon dioxide solubility in the deep eutectic solvent (1 ChCl+ 3 triethylene glycol) and modeling by the CPA EoS, J. Mol. Liq. 330 (2021) 115647.
[19] D.M. Makarov, Y.A. Fadeeva, V.A. Golubev, A.M. Kolker, Designing deep eutectic solvents for efficient CO2 capture: a data-driven screening approach, Sep. Purif. Technol. 325 (2023) 124614.
[20] F. Luo, X. Liu, S. Chen, Y. Song, X. Yi, C. Xue, L. Sun, J. Li, Comprehensive evaluation of a deep eutectic solvent based CO2 capture process through experiment and simulation, ACS Sustain. Chem. Eng. 9 (2021) 10250–10265.
[21] I. Zahrina, Y.Azis Sunarno, F. Aisha, Natural deep eutectic solvents as green and homogeneous catalysts for the glycerolysis of stearic acid: catalytic activity and kinetic studies, Results Eng. 23 (2024) 102801.
[22] R. Haghbakhsh, M. Keshtkar, A. Shariati, S. Raeissi, A comprehensive experimental and modeling study on CO2 solubilities in the deep eutectic solvent based on choline chloride and butane-1, 2-diol, Fluid Ph. Equilib. 561 (2022) 113535.
[23] R. Haghbakhsh, M. Keshtkar, A. Shariati, S. Raeissi, A study on carbon dioxide solubility in the deep eutectic solvent (1 sodium bromide+ 6 ethylene glycol): experimental and modeling by the SRK and CPA EoS, J. Chem. Thermodyn. 178 (2023) 106971.
[24] A. Al-Bodour, N. Alomari, A. Gutiérrez, S. Aparicio, M. Atilhan, Exploring the thermophysical properties of natural deep eutectic solvents for gas capture applications: a comprehensive review, Green Chem. Eng. 5 (2024) 307–338.
[25] G. Soave, Equilibrium constants from a modified Redlich-Kwong equation of state, Chem. Eng. Sci. 27 (1972) 1197–1203.
[26] T.Y. Kwak, G.A. Mansoori, Van der Waals mixing rules for cubic equations of state. Applications for supercritical fluid extraction modelling, Chem. Eng. Sci. 41 (1986) 1303–1309.
[27] H. Orbey, S.I. Sandler, On the combination of equation of state and excess free energy models, Fluid Ph. Equilib. 111 (1995) 53–70.
[28] D.S.H. Wong, S.I. Sandler, A theoretically correct mixing rule for cubic equations of state, AIChE J. 38 (1992) 671–680.
[29] M.L. Michelsen, A modified Huron-Vidal mixing rule for cubic equations of state, Fluid Ph. Equilib. 60 (1990) 213–219.
[30] K. Parvaneh, A. Rasoolzadeh, A. Shariati, Modeling the phase behavior of refrigerants with ionic liquids using the QC-PC-SAFT equation of state, J. Mol. Liq. 274 (2019) 497–504.
[31] A. Rasoolzadeh, S. Raeissi, A. Shariati, C.J. Peters, Experimental measurements and thermodynamic modeling of high-pressure propane solubility in triethylene glycol, J. Supercrit. Fluids 163 (2020) 104881.
[32] A. Rasoolzadeh, S. Raeissi, A. Shariati, C.J. Peters, Experimental measurement and thermodynamic modeling of methane solubility in triethylene glycol within the temperature range of 343.16–444.95 K, J. Chem. Eng. Data 65 (2020) 3866–3874.
[33] M.A. Sedghamiz, S. Raeissi, Physical properties of deep eutectic solvents formed by the sodium halide salts and ethylene glycol, and their mixtures with water, J. Mol. Liq. 269 (2018) 694–702.
[34] B.E. Poling, J.M. Prausnitz, J.P. O'connell, Properties of Gases and Liquids, McGraw-Hill Education, 2001.
[35] J.M. Prausnitz, R.N. Lichtenthaler, E.G. De Azevedo, Molecular Thermodynamics of Fluid-Phase Equilibria, Pearson Education, 1998.
[36] J.M. Smith, H.C. Van Ness, M.M. Abbott, Introduction to Chemical Engineering Thermodynamics, 7th ed., Mc-Graw Hill, New York, 2005.
[37] G. Li, D. Deng, Y. Chen, H. Shan, N. Ai, Solubilities and thermodynamic properties of CO2 in choline-chloride based deep eutectic solvents, J. Chem. Thermodyn. 75 (2014) 58–62.
[38] H. Ghaedi, M. Ayoub, S. Sufian, A.M. Shariff, S.M. Hailegiorgis, S.N. Khan, CO2 capture with the help of phosphonium-based deep eutectic solvents, J. Mol. Liq. 243 (2017) 564–571.
[39] K.A. Kurnia, F. Harris, C.D. Wilfred, M.I.A. Mutalib, T. Murugesan, Thermodynamic properties of CO2 absorption in hydroxyl ammonium ionic liquids at pressures of (100−1600) kPa, J. Chem. Thermodyn. 41 (2009) 1069–1073.
[40] R.H. Perry, D.W. Green, Perry's Chemical Engineers' Handbook, 9th Edition, 2018, p. sl.
[41] E. Mazandarani, A.H. Jalili, B. Adib, K. Tahvildari, A comparative study on the solubility of CH_3SH and H_2S in imidazolium-based ionic liquids: a connectionist approach between free volume and thermodynamics, Sep. Purif. Technol. 353 (2025) 128555.
[42] A.H. Jalili, A. Mehdizadeh, A.N. Ahmadi, A.T. Zoghi, M. Shokouhi, Solubility behavior of CO_2 and H_2S in 1-benzyl-3-methylimidazolium bis (trifluoromethylsulfonyl)imide ionic liquid, J. Chem. Thermodyn. 167 (2022) 106721.